Electronic Supplementary File for:

γ-FeO(OH) with Multi-surface Terminations Intrinsically Active for Electrocatalytic Oxygen Evolution Reaction

Laxmikanta Mallick,‡ Anubha Rajput,‡ Mrinal Kanti Adak, Avinava Kundu, Pratigya Choudhary Biswarup Chakraborty*

Department of Chemistry, Indian Institute of Technology Delhi, Hauz Khas, 110016, New Delhi, India

***E-mail: cbiswarup@chemistry.iitd.ac.in**

‡**These authors contributed equally to this work**

Characterization and Analysis Methods

1.1. Powder X-ray diffraction (PXRD)

The as-synthesized crystalline and amorphous α-and γ-FeO(OH) were characterized by powder x-ray diffraction on Bruker D8 Advance X-ray diffractometer equipped with Cu Kα (Kα1 = 1.540598 Å, Kα2 = 1.544426 Å, Kα ratio 0.5, Kαav = 1.541874Å) X-ray tubes.

1.2. Fourier Transform Infrared spectroscopy (FTIR)

The FTIR of crystalline and amorphous α-and γ-FeO(OH) was characterized by Nicolet, Protege 460 by making pellet. The pellet was made by mixing small amount of KBr with minute quantity of the sample

1.3. Raman spectroscopy

Raman spectroscopy was analyzed by micro-Raman spectrometer model (Renishaw plc, Old Town, Wotton-under-Edge, Gloucestershire, GL 12 7 DW, United Kingdom), in which 514nm Argon laser was used.

1.4. Field Emission Scanning Electron Microscope (FESEM)

The field emission scanning electron microscopy (FESEM), and the Energy-dispersive X-ray spectroscopy (EDX) techniques were used for mapping and elemental analysis was done by JSM-IT300HR, JEOL instrument.

1.5. High-resolution Transmission Electron Microscopy (HRTEM)

The synthesized crystalline and amorphous α-and γ-FeO(OH) were further characterized by high-resolution transmission electron microscopy (HRTEM). HRTEM images and selected area electron diffraction (SAED) patterns were performed using a Thermo Fischer Technik microscope working at accelerated voltage 200 kV. TEM grids for crystalline and amorphous α-and γ-FeO(OH) were prepared on the 200-mesh carbon-coated Cu grids [TED PELLA, INC.] with the help of their respective dilute suspensions in HPLC grade acetone (Merck, India).

1.6. X-ray photoelectron spectroscopy (XPS)

The X-ray photoelectron spectroscopy (XPS) measurements were conducted through omicron nanotechnology, Oxford Instrument Germany, equipped with an aluminum monochromator

with an aluminium source (Al Kα radiation hν =1486.7eV). The operational voltage and current of the instrument were at 15 kV and 15 mA.

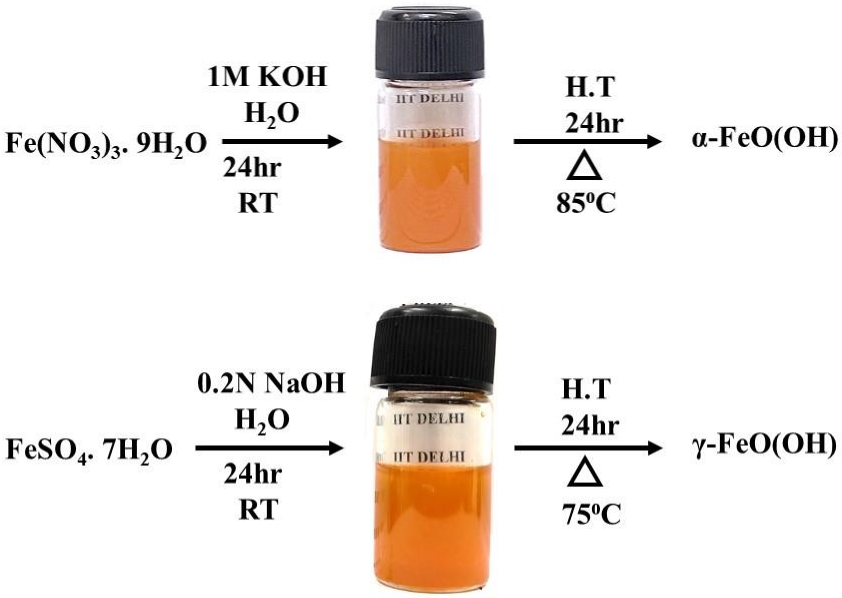

Figure S1. Preparation of α-FeO(OH) (top) and γ-FeO(OH) (bottom) via hydrothermal route.

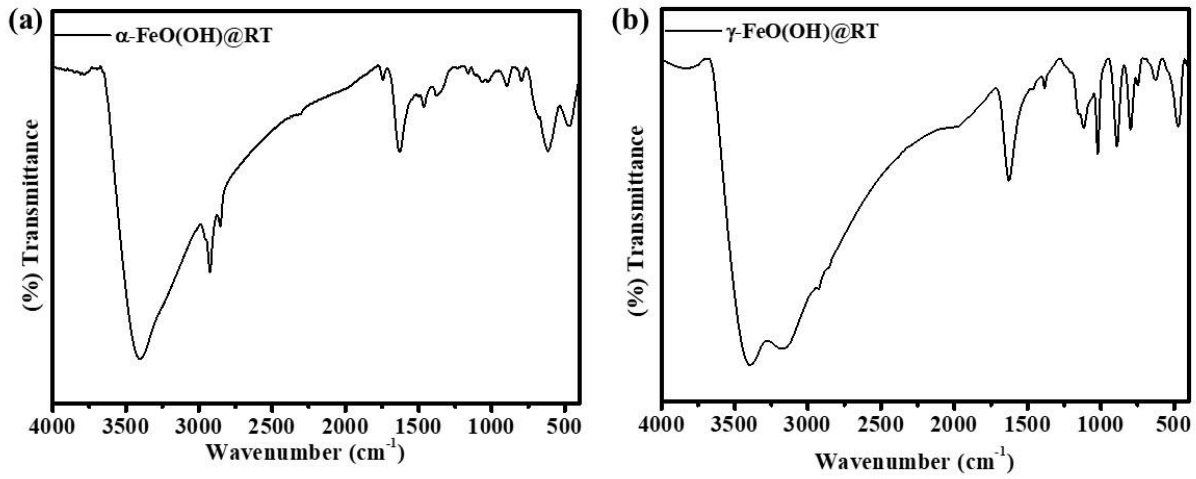

Figure S2. FTIR spectra of (a) α-FeO(OH)@RT and (b) γ -FeO(OH)@RT.

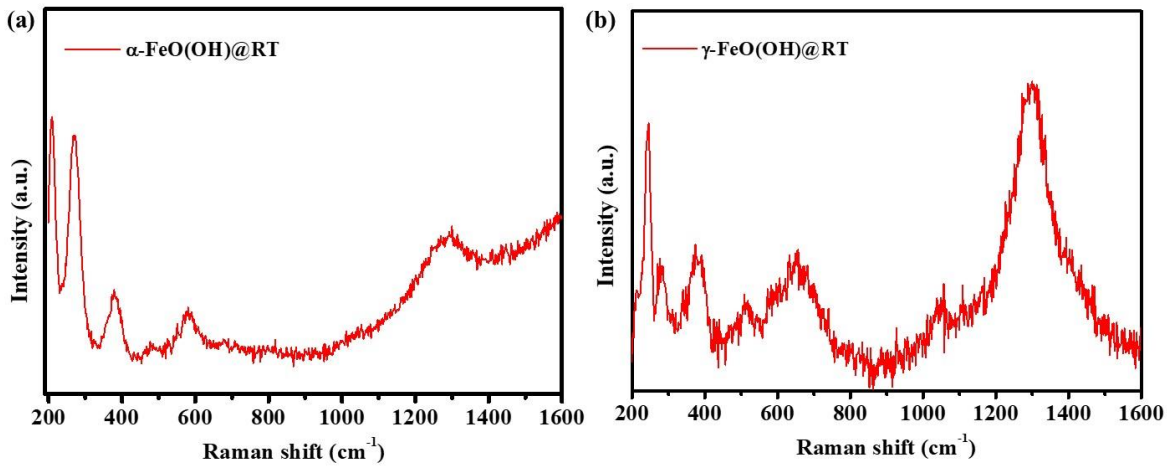

Figure S3. Raman spectra of (a) α-FeO(OH)@RT and (b) γ -FeO(OH)@RT.

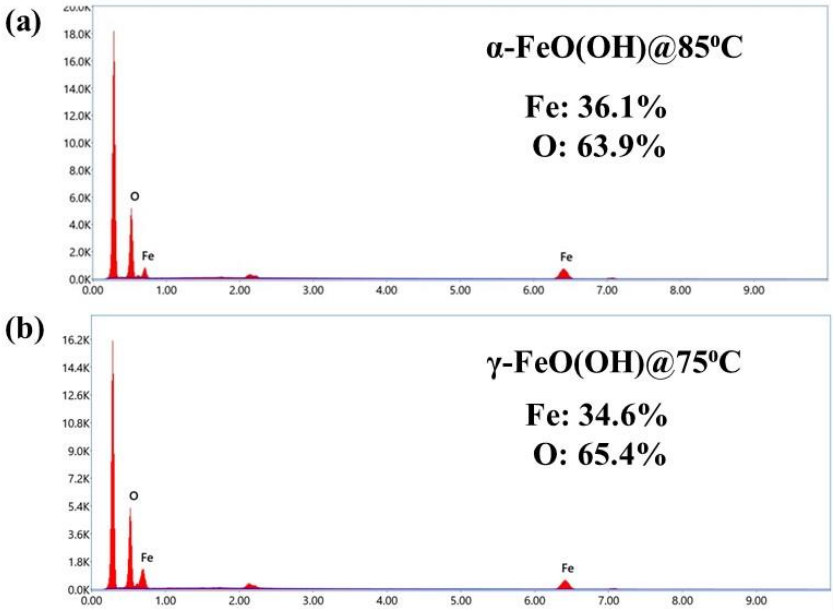

Figure S4. EDS spectra of the as-prepared (a) α-FeO(OH)@85ºC (b) γ-FeO(OH)@75ºC. The atomic ratio of Fe and O atoms was 1:2.

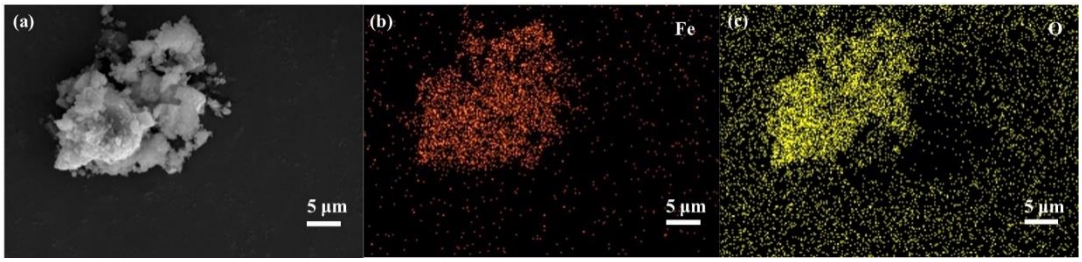

Figure S5. (a) FESEM image of α-FeO(OH)@RT. Elemental mapping of (b) O-atom (c) Fe-atom.

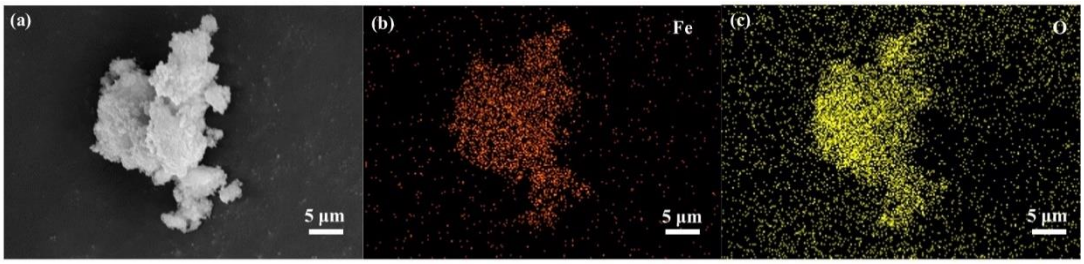

Figure S6. (a) FESEM image of γ-FeO(OH)@RT. Elemental Mapping of (b) O-atom (c) Fe-atom.

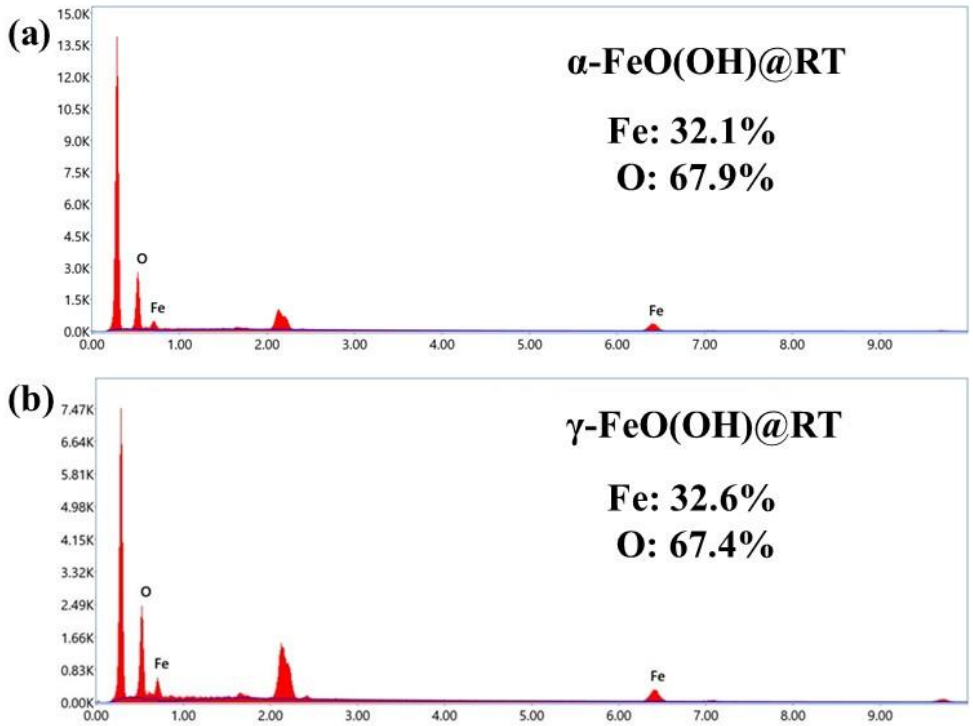

Figure S7. EDS spectra of the as-prepared (a) α-FeO(OH)@RT (b) γ-FeO(OH)@RT. The atomic ratio of Fe and O atoms was 1:2.

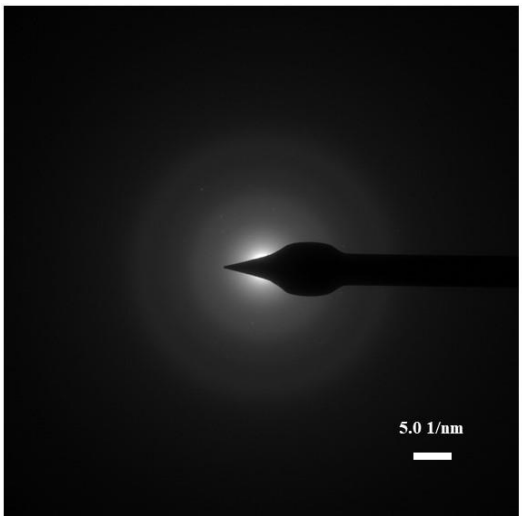

Figure S8. SAED pattern of amorphous α-FeO(OH)@RT.

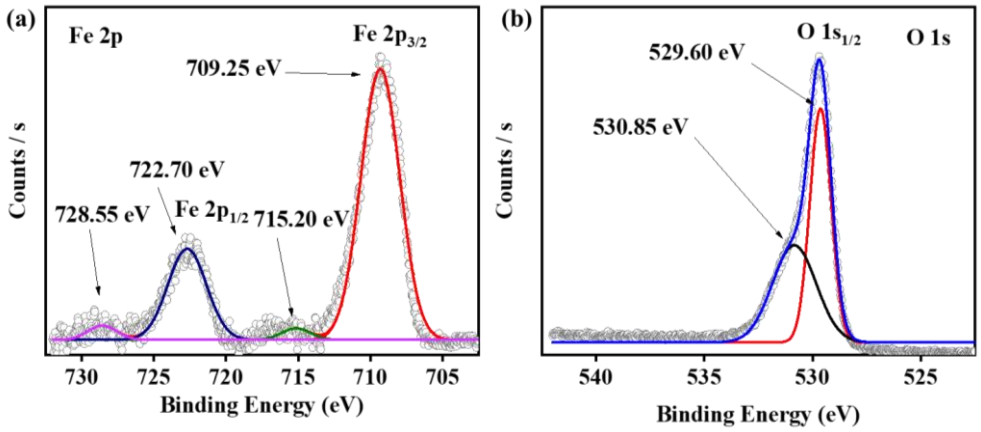

Figure S9. XPS study with α-FeO(OH)@RT showing the high resolution (a) Fe 2p scan (b) O 1s scan.

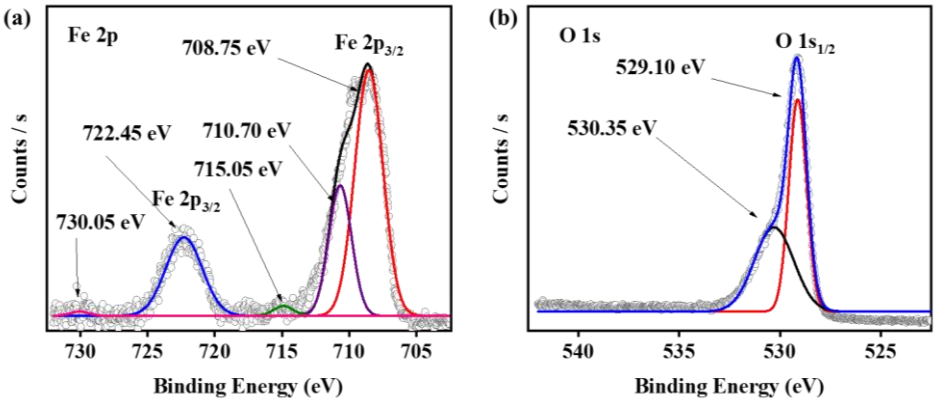

Figure S10: XPS study with γ-FeO(OH)@RT showing the high resolution (a) Fe 2p scan (b) O 1s scan.

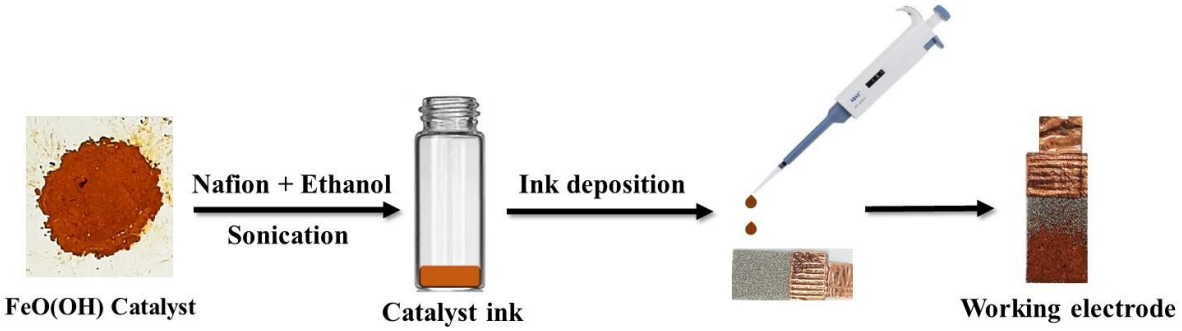

Figure S11. Preparation of electrode with FeO(OH) catalysts on NF electrode.

Table S1. Overpotentials (η) recorded for OER study with FeO(OH) iron-based oxyhydroxide anodes reported earlier as the anode in 1 M KOH.

Anode material	Substrate	Ŋ(mV)@10 mA cm^{-2}	Reference
FeO(OH)	NF	428	[1]
FeO(OH)	NF	290	[2]
FeO(OH)(Se)	IF	287	[3]
Fe_2O_3/CNT	GC	383	[4]
γ-Fe_2O_3-CNT	GC	340	[5]
CNT/FeO(OH)	CC	250	[6]
FeO(OH) nanosheet	NF	390	[7]
FeO(OH)	NF	280	[8]
NiFeOX	GC	350	[9]
Ni-FeO(OH)	Fe-foil	274	[1]
$Co_{0.54}Fe_{0.46}O(OH)$	GC	390	[10]
RGO/Ni-FeO(OH)	FTO	260	[11]
FeO(OH)/CeO_2	NF	250	[12]
FeO(OH)@NG	$Fe_{78}Si_9B_{13}$ amorphous alloy	240	[13]
FeO(OH)/LDH	GCDE	174	[14]
Se doped FeO(OH)	NF	348@500 mA cm^{-2}	[3]
$NiCo_2S_4$/FeO(OH)	CC	200	[15]
β/δ-FeO(OH)	NF	180 mV	[16]
FeO(OH)@CNTs	NF	206	[17]
FeO(OH) powder	NF	441	[17]
FeO(OH)/Co/FeO(OH) HNTAs	NF	350	[18]
γ-FeO(OH)	NF	286	[19]
α-FeO(OH)	FTO	620	[20]
FeO(OH)/Ni_3N	CC	244	[21]
δ-FeO(OH)	NF	292	[16]
FeO(OH)	IF	428	[1]
δ-FeO(OH)	NF	290	[22]
F-modified β-FeO(OH)		360	[23]

Abbreviations: NF = Nickel Foam; CC = Carbon Cloth; GC = Glassy Carbon electrode; IF = Iron Foam; CP = Carbon fibre Paper; SS = Stainless Steel; FTO = Fluorine doped Tin Oxide; NC = N-doped Carbon; GCDE = glassy carbon disk electrode

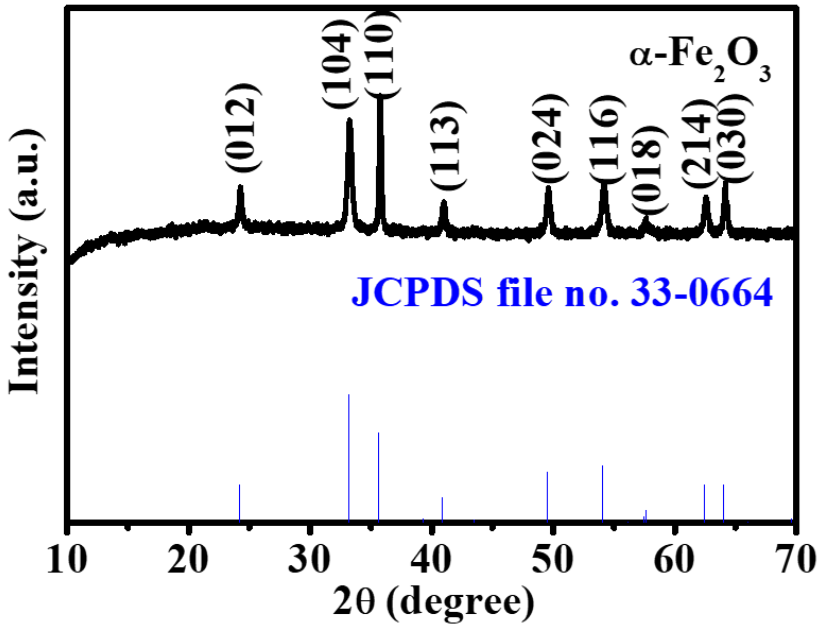

Figure S12. Powder X-ray diffraction spectrum of α-Fe_2O_3 (black curve) prepared herein and indexing of the reflections to the JCPDS 33-0664 (blue bars).

Table S2. Mass loading of the iron materials on NF.

Material	Mass loading (mg)
γ-FeO(OH)@RT	7.4
γ-FeO(OH)@50ºC	5.8
γ-FeO(OH)@75ºC	7.3
α-FeO(OH)@RT	9.1
α-FeO(OH)@50ºC	7.2
α-FeO(OH)@85ºC	6.1

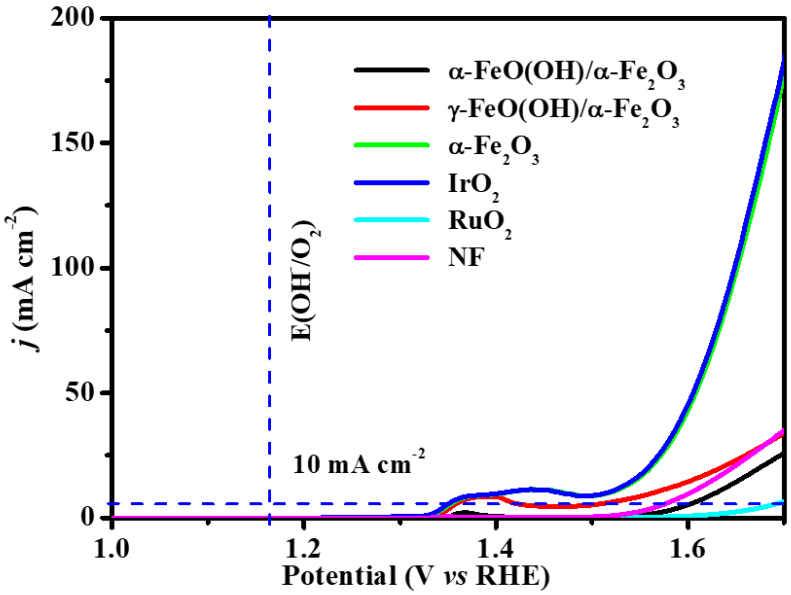

Figure S13. Linear sweep voltammetry of α-Fe_2O_3 and mixed phase α-FeO(OH)/α-Fe_2O_3 and γ-FeO(OH)/α-Fe_2O_3 materials in comparison to RuO_2 and IrO_2.

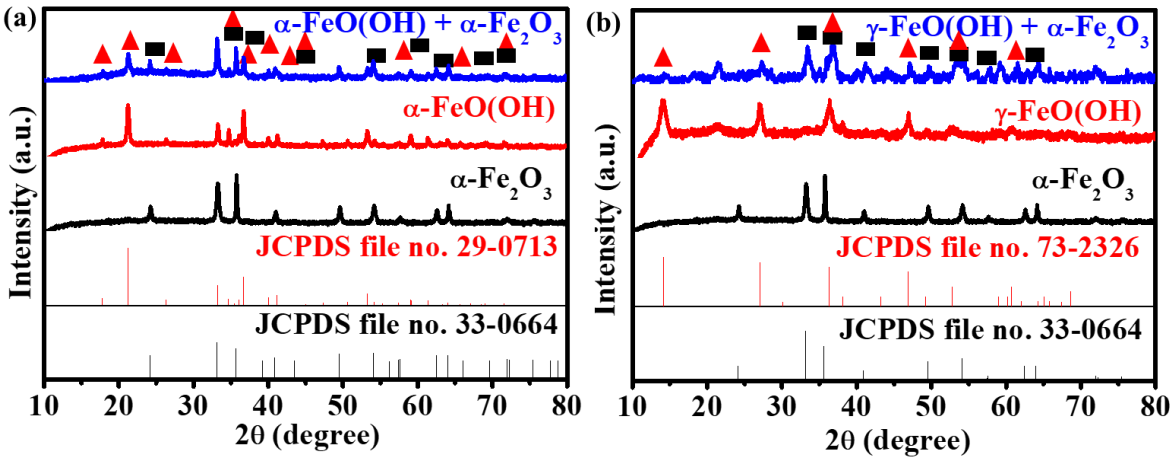

Figure S14. Powder X-ray diffraction spectra of (a) α-FeO(OH)/α-Fe_2O_3 (b) γ-FeO(OH)/ α-Fe_2O_3 along with the indexing of peaks with reference to the JCPDS cards.

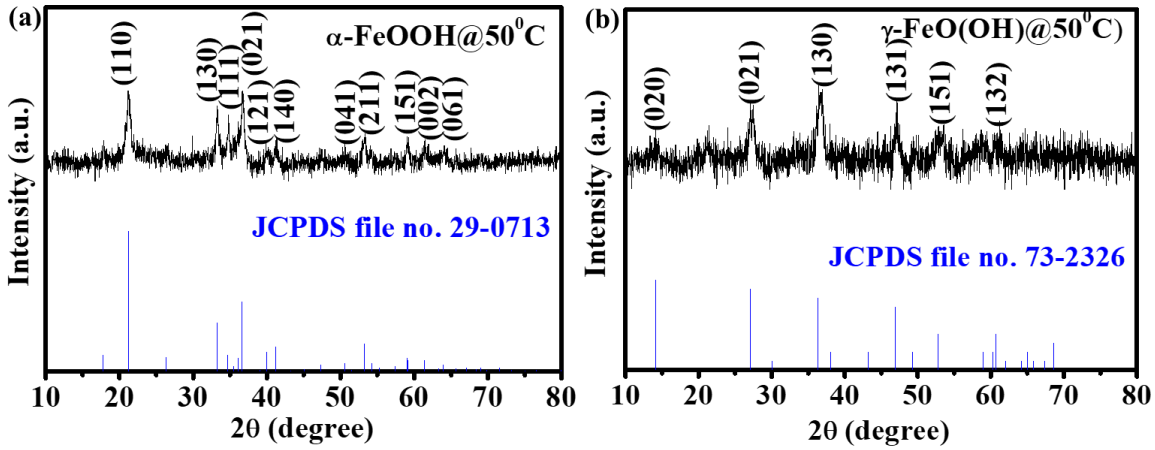

Figure S15. Powder X-ray diffraction spectra of partially crystalline (a) α-FeO(OH)@50ºC and (b) γ-FeO(OH)@50ºC.

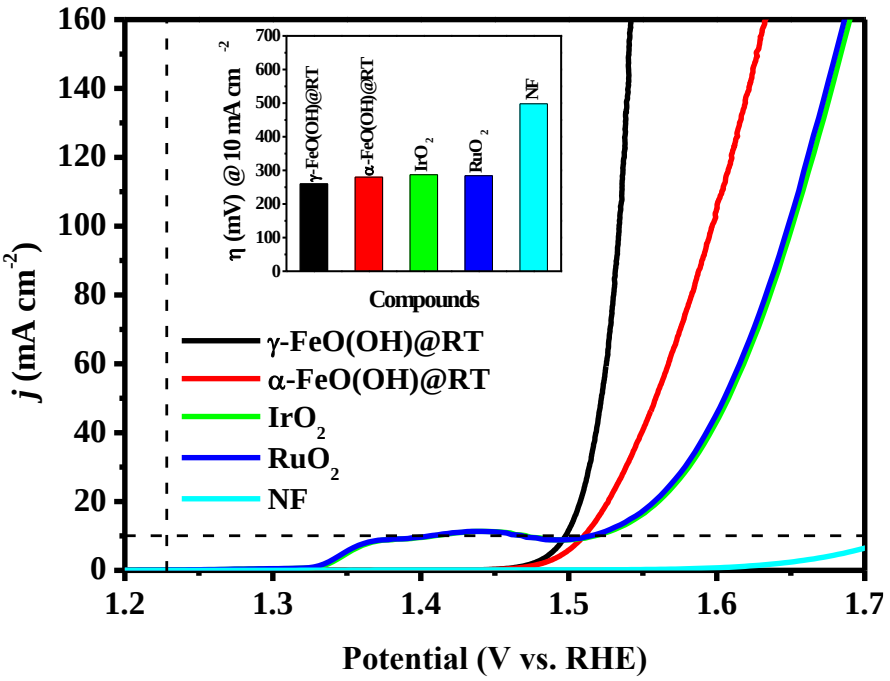

Figure S16. Polarization curves recorded with the working electrodes prepared with γ-FeO(OH)@RT, α-FeO(OH)@RT, IrO_2, RuO_2 deposited on 1 cm^2 NF surface and bare NF using 1 M KOH solution and in a sweep rate of 1 mV s^{-1}. (Inset) Overpotential calculated from the LSV plots of γ-FeO(OH)@RT, α-FeO(OH)@RT, IrO_2, RuO_2, and bare NF at a current density of 10 mA cm^{-2}.

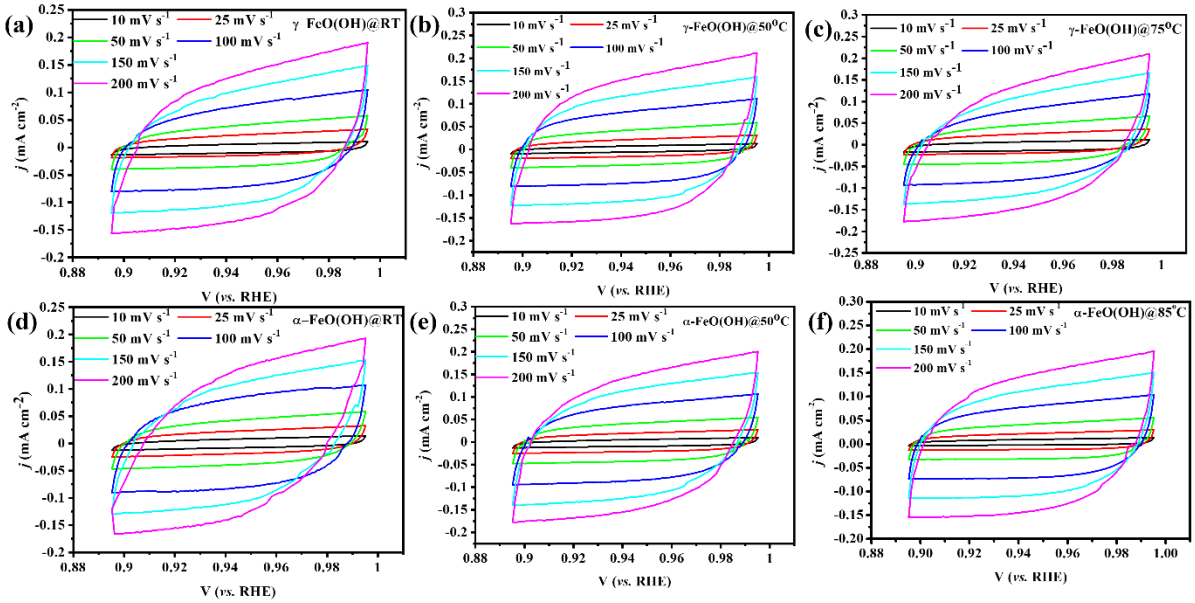

Figure S17. The ECSA plot used to determine the double-layer capacitance (C_{dl}) of different catalysts. CV scans in the non-Faradaic potential range (-0.05 – 0.05V) at scan rates of 10 mV s^{-1}, 25 mV s^{-1}, 50 mV s^{-1}, 100 mV s^{-1}, 150 mV s^{-1} and 200 mV s^{-1}. The ECSA plots of (a) γ-FeO(OH)@RT (b) γ-FeO(OH)@50°C (c) γ-FeO(OH)@75°C (d) α-FeO(OH)@RT (e) α-FeO(OH)@50°C (f) α-FeO(OH)@85°C.

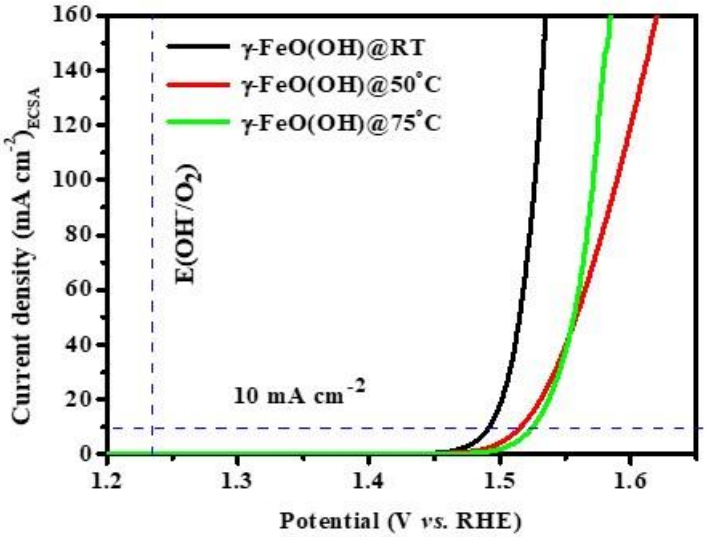

Figure S18. ECSA normalized activity of γ-FeO(OH)@RT, γ-FeO(OH)@50°C, γ-FeO(OH)@75°C.

Table S3. Comparison of TOF of, γ-FeO(OH)@RT γ-FeO(OH)@50ºC γ-FeO(OH)@85ºC, α-FeO(OH)@RT, α-FeO(OH)@50ºC, and α-FeO(OH)@85ºC.

Material	Turn over frequency
γ-FeO(OH)@RT	1.6 x 10^{-3} s^{-1}
γ-FeO(OH)@50ºC	0.59 x 10^{-3} s^{-1}
γ-FeO(OH)@75ºC	0.3 x 10^{-3} s^{-1}
α-FeO(OH)@RT	0.845 x 10^{-3} s^{-1}
α-FeO(OH)@50ºC	0.436 x 10^{-3} s^{-1}
α-FeO(OH)@85ºC	0.343 x 10^{-3} s^{-1}

Table S4. R_s value obtained from the Nyquist plot (Figure 9a and 9b).

Material	*R_s (Ω)*
γ-FeO(OH)@RT	*2.12 ± 0.2*
γ-FeO(OH)@50ºC	*1.96 ± 0.3*
γ-FeO(OH)@75ºC	*2.21 ± 0.2*
α-FeO(OH)@RT	*2.13 ± 0.1*
α-FeO(OH)@50ºC	*2.01 ± 0.2*
α-FeO(OH)@85ºC	*2.53 ± 0.2*

Reference:

(1) Zou, J.; Peleckis, G.; Lee, C.-Y.; Wallace, G. G. Facile Electrochemical Synthesis of Ultrathin Iron Oxyhydroxide Nanosheets for the Oxygen Evolution Reaction. *Chem. Commun.* **2019**, *55* (60), 8808–8811.

(2) Babar, P. T.; Pawar, B. S.; Lokhande, A. C.; Gang, M. G.; Jang, J. S.; Suryawanshi, M. P.; Pawar, S. M.; Kim, J. H. Annealing Temperature Dependent Catalytic Water Oxidation Activity of Iron Oxyhydroxide Thin Films. *J. energy Chem.* **2017**, *26* (4), 757–761.

(3) Niu, S.; Jiang, W.-J.; Wei, Z.; Tang, T.; Ma, J.; Hu, J.-S.; Wan, L.-J. Se-Doping Activates FeOOH for Cost-Effective and Efficient Electrochemical Water Oxidation. *J. Am. Chem. Soc.* **2019**, *141* (17), 7005–7013.

(4) Bandal, H. A.; Jadhav, A. R.; Chaugule, A. A.; Chung, W. J.; Kim, H. Fe2O3 Hollow Nanorods/CNT Composites as an Efficient Electrocatalyst for Oxygen Evolution Reaction. *Electrochim. Acta* **2016**, *222*, 1316–1325.

(5) Tavakkoli, M.; Kallio, T.; Reynaud, O.; Nasibulin, A. G.; Sainio, J.; Jiang, H.; Kauppinen, E.

I.; Laasonen, K. Maghemite Nanoparticles Decorated on Carbon Nanotubes as Efficient Electrocatalysts for the Oxygen Evolution Reaction. *J. Mater. Chem. A* **2016**, *4* (14), 5216–5222.

(6) Zhang, Y.; Jia, G.; Wang, H.; Ouyang, B.; Rawat, R. S.; Fan, H. J. Ultrathin CNTs@ FeOOH Nanoflake Core/Shell Networks as Efficient Electrocatalysts for the Oxygen Evolution Reaction. *Mater. Chem. Front.* **2017**, *1* (4), 709–715.

(7) Lee, J.; Lee, H.; Lim, B. Chemical Transformation of Iron Alkoxide Nanosheets to FeOOH Nanoparticles for Highly Active and Stable Oxygen Evolution Electrocatalysts. *J. Ind. Eng. Chem.* **2018**, *58*, 100–104.

(8) Zhang, C.; Zhang, B.; Li, Z.; Hao, J. Deep Eutectic Solvent-Mediated Hierarchically Structured Fe-Based Organic–Inorganic Hybrid Catalyst for Oxygen Evolution Reaction. *ACS Appl. Energy Mater.* **2019**, *2* (5), 3343–3351.

(9) McCrory, C. C. L.; Jung, S.; Peters, J. C.; Jaramillo, T. F. Benchmarking Heterogeneous Electrocatalysts for the Oxygen Evolution Reaction. *J. Am. Chem. Soc.* **2013**, *135* (45), 16977–16987.

(10) Zhang, X.; An, L.; Yin, J.; Xi, P.; Zheng, Z.; Du, Y. Effective Construction of High-Quality Iron Oxy-Hydroxides and Co-Doped Iron Oxy-Hydroxides Nanostructures: Towards the Promising Oxygen Evolution Reaction Application. *Sci. Rep.* **2017**, *7* (1), 1–10.

(11) Zhang, X.; Zhang, B.; Liu, S.; Kang, H.; Kong, W.; Zhang, S.; Shen, Y.; Yang, B. RGO Modified Ni Doped FeOOH for Enhanced Electrochemical and Photoelectrochemical Water Oxidation. *Appl. Surf. Sci.* **2018**, *436*, 974–980.

(12) Feng, J.; Ye, S.; Xu, H.; Tong, Y.; Li, G. Design and Synthesis of FeOOH/CeO2 Heterolayered Nanotube Electrocatalysts for the Oxygen Evolution Reaction. *Adv. Mater.* **2016**, *28* (23), 4698–4703.

(13) Zhu, K. Z.; Liu, C. B.; Ye, X. K.; Wu, Y. A Study of Catalysis of Copper-Aluminium Hydrotalcite-like Compounds in the Phenol Hydroxylation. *Acta Chim. Sin.* **1998**, *56* (1), 36.

(14) Chen, J.; Zheng, F.; Zhang, S.-J.; Fisher, A.; Zhou, Y.; Wang, Z.; Li, Y.; Xu, B.-B.; Li, J.-T.; Sun, S.-G. Interfacial Interaction between FeOOH and Ni–Fe LDH to Modulate the Local Electronic Structure for Enhanced OER Electrocatalysis. *ACS Catal.* **2018**, *8* (12), 11342–11351.

(15) Li, X.; Kou, Z.; Xi, S.; Zang, W.; Yang, T.; Zhang, L.; Wang, J. Porous NiCo2S4/FeOOH

Nanowire Arrays with Rich Sulfide/Hydroxide Interfaces Enable High OER Activity. *Nano Energy* **2020**, *78*, 105230.

(16) Hu, J.; Li, S.; Chu, J.; Niu, S.; Wang, J.; Du, Y.; Li, Z.; Han, X.; Xu, P. Understanding the Phase-Induced Electrocatalytic Oxygen Evolution Reaction Activity on FeOOH Nanostructures. *ACS Catal.* **2019**, *9* (12), 10705–10711.

(17) Li, H.; Zhou, Q.; Liu, F.; Zhang, W.; Tan, Z.; Zhou, H.; Huang, Z.; Jiao, S.; Kuang, Y. Biomimetic Design of Ultrathin Edge-Riched FeOOH@ Carbon Nanotubes as High-Efficiency Electrocatalysts for Water Splitting. *Appl. Catal. B Environ.* **2019**, *255*, 117755.

(18) Feng, J.; Xu, H.; Dong, Y.; Ye, S.; Tong, Y.; Li, G. FeOOH/Co/FeOOH Hybrid Nanotube Arrays as High-performance Electrocatalysts for the Oxygen Evolution Reaction. *Angew. Chemie Int. Ed.* **2016**, *55* (11), 3694–3698.

(19) Wang, K.; Du, H.; He, S.; Liu, L.; Yang, K.; Sun, J.; Liu, Y.; Du, Z.; Xie, L.; Ai, W. Kinetically Controlled, Scalable Synthesis of Γ-FeOOH Nanosheet Arrays on Nickel Foam toward Efficient Oxygen Evolution: The Key Role of In-situ-generated Γ-NiOOH. *Adv. Mater.* **2021**, *33* (11), 2005587.

(20) Chakraborty, B.; Beltrán-Suito, R.; Hausmann, J. N.; Garai, S.; Driess, M.; Menezes, P. W. Enabling Iron-Based Highly Effective Electrochemical Water-Splitting and Selective Oxygenation of Organic Substrates through In Situ Surface Modification of Intermetallic Iron Stannide Precatalyst. *Adv. Energy Mater.* **2020**, *10* (30), 2001377.

(21) Guan, J.; Li, C.; Zhao, J.; Yang, Y.; Zhou, W.; Wang, Y.; Li, G.-R. FeOOH-Enhanced Bifunctionality in Ni3N Nanotube Arrays for Water Splitting. *Appl. Catal. B Environ.* **2020**, *269*, 118600.

(22) Liu, B.; Wang, Y.; Peng, H.; Yang, R.; Jiang, Z.; Zhou, X.; Lee, C.; Zhao, H.; Zhang, W. Iron Vacancies Induced Bifunctionality in Ultrathin Feroxyhyte Nanosheets for Overall Water Splitting. *Adv. Mater.* **2018**, *30* (36), 1803144.

(23) Chen, G.-F.; Luo, Y.; Ding, L.-X.; Wang, H. Low-Voltage Electrolytic Hydrogen Production Derived from Efficient Water and Ethanol Oxidation on Fluorine-Modified FeOOH Anode. *ACS Catal.* **2018**, *8* (1), 526–530.